

RESEARCH ON A RICE FIELD METHANE DETECTION SYSTEM USING HOLLOW-CORE PHOTONIC CRYSTAL FIBRE BASED ON TDLAS TECHNIQUE

基于 TDLAS 技术的空心光子晶体光纤稻田甲烷气体检测系统研究

Bin LI* ¹⁾, Ruotong LIU¹⁾, Guangfei SHANG¹⁾, Lihui ZHANG¹⁾, Chenghao HAN²⁾, Yitong HUANG¹⁾ ¹

¹⁾ School of Electrical & Computer Engineering, Jilin Jianzhu University, Changchun 130012, P.R. China;

²⁾ School of Emergency Science and Engineering, Jilin Jianzhu University, Changchun 130012, P.R. China;

Tel: +86-043184566184; E-mail: libin@jlju.edu.cn; 870731919@qq.com;

DOI: <https://doi.org/10.35633/inmateh-75-66>

Keywords: Methane detection; rice field; DFB laser diode; infrared absorption

ABSTRACT

A methane gas detection system has been developed based on the infrared absorption method. The system can be deployed in dry rice field for real-time detection. It consists of self-developed circuits and essential optical parts. A distributed feedback laser has been chosen as the optical source of the system. Hollow-core photonic crystal fibre is also applied as a part of the gas cell. The major circuit boards include laser driver circuit, laser temperature control circuit, digital lock-in amplifier circuit and linear power circuit. The laser diode can be effectively controlled by using the above circuits. The laser driving current step is 1 mA and the temperature fluctuation is less than ± 0.02 °C. Based on the TDLAS technique, spectroscopy test shows that the proposed laser driving circuits has accurate control capability. The detection error is about 2.3% by performing the full-scale detection experiments. Further gas detection experiments using standard gas under 600 ppm also demonstrate the effectiveness and stability of the proposed system. By replacing the optical source and essential driving circuits of the system, the system can be applied to detect other trace gases.

摘要

开发了一种基于红外光谱吸收法的甲烷气体检测系统。研制的系统能够应用在旱稻田中进行实时气体检测。它由自主开发的电路和相关光学部件组成。分布式反馈激光器作为光源，空心光子晶体光纤作为气室的一部分。系统中主要电路板包括激光器的驱动电路、激光器的温度控制电路、数字锁向放大器电路和线性电源电路。使用上述电路可以有效地控制激光二极管。激光驱动电流步长为 1 mA，其温度波动可以限制在 ± 0.02 °C 的范围内。基于 TDLAS 技术，光谱测试表明，所提出的激光驱动电路具有精确的控制能力。通过进行全量程的气体检测实验，检测误差约为 2.3%。进一步使用 600 ppm 以下的标准气体进行气体检测实验也证明了文章中提出系统的稳定性、有效性。通过更换系统的光源和基本驱动电路，该系统可以应用于其他痕量气体的检测。

INTRODUCTION

Rice as an important food crop is widely cultivated in China and many regions around the world. However, in recent years, the methane gas released from paddy fields has attracted the attention of many researchers (Jikun H. et al., 2014; Mujiyo M. et al., 2017; Xie B.H. et al., 2010). It is widely researched that CH₄ is a kind of important greenhouse gas and it is 28 times higher than carbon dioxide with a global warming potential (Ma J.L. et al., 2019; Palmer P.I. et al., 2021; Rajasekar P. et al., 2022; Rizzo et al., 2015). According to studies in the past years, the methane gas released from rice fields are increasing for numerous reasons (Bai Y. et al., 2023; Xu X.Y. et al., 2020). In this way, it is important to develop advanced and reliable sensors for monitoring methane gas in rice fields for purposes including environmental protection and sustainability.

Traditional methods of methane detection in rice field such as chamber technique has some drawbacks. The measurement accuracy of chamber technique is good. And this method is widely used for many years. However, it is not efficient in the real-time detection and monitoring of large areas of rice fields. Other traditional methods such as micrometeorological technique and isotope method, also have drawbacks including unstable accuracy and complex requirements in the sensing process (Arianti F.D. et al. 2023; Gao Z.R. et al., 2018; Zhang G.B. et al., 2014; Zhang G.B. et al., 2015). Therefore, it is essential to apply advanced methods for high-precision and large-scale monitoring of methane gas in rice fields.

¹ Bin Li, Prof.; Ruotong Liu, Stud.; Guangfei Shang, Stud.; Lihui Zhang, Prof.; Chenghao Han, Prof.; Yitong Huang, Stud.

The infrared spectral absorption method is an advanced optical technique to monitor trace gases which has been studied by many researchers. In 2021, Catia L. etc. proposed their work with an immunosensor for achieving fast and highly sensitive detection of cortisol based on plasmonic tilted fiber (Catia L. et al., 2021). In 2023, Maxime L. etc. proposed an electro-plasmonic biosensor for attracting cells and proteins by migration of controlled biomolecular. The sensor is on the surface of a probe linked with fiber (Maxime L. et al., 2023). Compared with traditional detection methods, the infrared spectral absorption method is characterized by high precision and rapid response. At the same time, this method has strong selectivity and is capable of monitoring specific gases for a long time in an open space. Different types of optical fibers are widely used in these detection systems (Bai Y.R. et al., 2021; Dar S.A. et al., 2020; Davis N.M. et al., 2016; Jiao Y.X. et al., 2021). Hollow-core photonic crystal fiber (HC-PCF) can be used not only for the transmission of optical signals but also as a part of the gas cell, enabling the target gas to come into contact with the light beam so as to achieve spectral absorption. It has been applied to replace gas chambers to achieve effective detection of target gas. Meanwhile, distributed feedback (DFB) laser diode has the characteristics of narrow linewidth and wavelength tunability. It can be linked with HC-PCF and commercial communication fiber to achieve the transmission of optical signals over long distances. Therefore, HC-PCF and DFB laser diode are suitable for the detection system based on infrared spectral absorption method.

In this paper, a highly integrated CH₄ sensing system is proposed. In the system, DFB laser diode and HC-PCF have been applied with other self-developed key modules. The TDLAS technique has been adopted as the core detection method in this system to perform gas sensing experiments. In this way, DFB laser diode has been chosen as the optical source in this system with other relevant optical parts such as fiber optic beam splitter and photodiodes. Compared to other commercial light sources such as QCL lasers, DFB laser diode has the advantage including effective tunable ability and lower heat generation. Therefore, remote detection of target gas can be achieved by its working features. The emitting light beam can be controlled and be modulated to meet the requirements of the TDLAS technique. Compared to our earlier research (Bin L. et al., 2018), the hardware part has been upgraded by using more powerful chips. And the software part has been upgraded by optimizing the control algorithm especially for laser temperature controlling circuit. This part has been updated in many ways. The photoelectric conversion circuit uses InGaAs photodiodes with a higher cost-performance ratio, which reduces the cost while ensuring the conversion performance. Meanwhile, second harmonic signals can be extracted for gas detection by using the technique of wavelength modulation spectroscopy (WMS). The proposed system can be deployed to perform CH₄ detection in large-scale rice fields remotely.

SYSTEM STRUCTURE AND DETECTION THEORY

System structure

The functional diagram of the proposed CH₄ sensing system is shown in Fig. 1. On the left side of Fig. 1 is the independently integrated detection system, which includes optical devices and electronic devices. The acrylic box on the right side of Fig. 1 is the gas cell of the detection system. It is placed in a dry paddy field for detection. Firstly, the detection system on the left side is integrated in an instrument case and can be placed near the measured area, and then communicates with the measured area through an optical fiber. This instrument has been proposed in our previous work. Then, the HC-PCF allows target gas spreads inside the fiber in order to be irradiated by the near infrared light beam. In this way, the gas absorption phenomenon can occur. The optical signal after coming into contact with the measured gas returns to the integrated detection instrument through the optical fiber, and the lost optical signal can be used to calculate the concentration of the gas.

The proposed detection instrument contains many key electrical and optical modules. All the calculation work is completed by the main control chip which is a Digital Signal Processor (DSP), including generating modulation signals, generating laser control instructions, and calculating the gas concentration, etc. The modulation signal includes ramp wave and sine wave. After the modulation signal of the laser is output by the DSP, the laser is driven by a ramp wave signal. It is generated by a high-performance Digital-to-Analog (DAC) chip which type is AD5541. Meanwhile, a Direct-Digital-Synthesizer (DDS) chip is applied to generate sine wave signal and the chip type is AD9851. With the signal modulation, a fiber optic beam splitter (FOBS) is used to divide the output signal of the DFB laser into two equal parts. One part enters the gas cell and undergoes an absorption reaction, and the other part has its light intensity reduced by an optical attenuator (OA). After photoelectric conversion which uses two InGaAs photodiodes, the difference between the two signals contains the information about the gas concentration. In this way, the subtraction of the absorbed signal

and the reference signal can be performed. In this system, it is sent digitally to the DSP by using an Analog-to-Digital (ADC) chip. Finally, the result of detection can be displayed or processed for further applications. The calculated data can be sent to a laptop via the UART port. And the gas information can be received by using software developed by LabVIEW to perform further analysis.

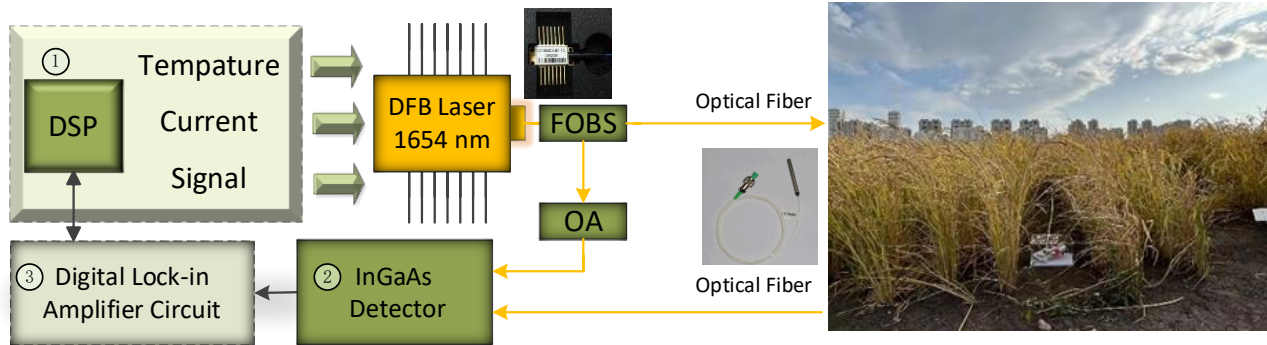


Fig. 1 - Block diagram of rice field methane gas detection system using TDLAS technique

Detection theory

Based on the TDLAS technique, the absorption line of CH₄ must be scanned across periodically in order to detect the optical loss. Fig. 2(a) shows the absorption spectrum of CH₄ around 1654 nm. And its absorption intensity is at the level of 10⁻²¹ cm⁻¹/(molecule cm⁻²). Therefore, in order to meet the requirement of detection, the selection of the laser is very important. In this system, a DFB laser is applied as the main light source of the detection system. Both DFB lasers and Quantum Cascade Laser (QCL) lasers are widely used in the field of gas detection. Compared with QCL lasers, DFB lasers are more likely to use optical fibers for long-distance signal transmission, which is applicable for the remote detection of methane gas in paddy fields. At the same time, DFB lasers are cheaper than QCL lasers, which also helps to carry out relevant experiments. The applied DFB laser has the center wavelength around 1654 nm as shown in Fig 2(d). In this infrared region, there are interfering gases such as H₂O and CO₂, which are also shown in Fig. 2 to demonstrate their absorption lines. It can be seen that their absorption intensity is much weaker than the intensity of CH₄. Their absorption intensity are 4 orders of magnitude lower than that of methane as shown in Fig. 2(b) and Fig. 2(c). Therefore, when detecting methane in this interval, water and carbon dioxide in the atmosphere hardly cause any interference. High selectivity is an advantage of the infrared spectroscopy method. When using traditional gas detection methods, it is very easy to be affected by interfering gases.

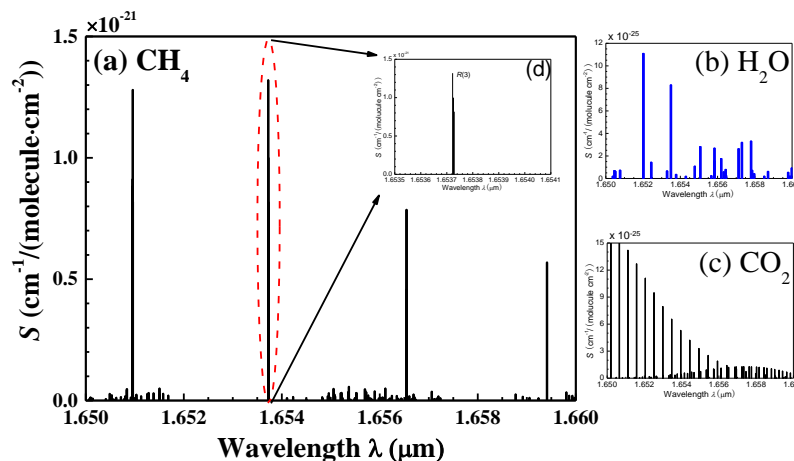


Fig. 2 - Absorption line selection of CH₄ (a) (d) and the absorption intensity of the interfering gas H₂O (b) and CO₂ (c) in this infrared region

The detection theory of absorption spectroscopy is governed by the Beer-Lambert law. The calculation is determined by the optical loss of spectral intensity (W/m²) while radiation interacts with gas molecules. The expression of the coefficient $\tau(\nu, t)$ is shown in Eq. (1). The transmitted intensity and the initial light intensity can be expressed as $I(\nu)$ and $I_0(\nu)$ respectively. The relationship can be seen as follows:

$$\tau(\nu, t) = \frac{I(\nu)}{I_0(\nu)} = \exp[-\alpha(\nu, t)LC] \tag{1}$$

where $\alpha(v, t)$ (cm^{-1}) in Eq. (1) is the absorption coefficient at frequency v (cm^{-1}). In this equation, C is the mole fraction of the target gas and L is the effective optical path length. Based on TDLAS and WMS technique, the DFB laser is tuned by a low-frequency repetitive ramp waveform with the period of T_{ramp} . Meanwhile, a high-frequency sine wave signal is added to the ramp wave. Its angular frequency is expressed as ω_{sin} . The expressions of the above signals and the strength of the light source can be represented in Eq. (2), Eq. (3) and Eq. (4), respectively:

$$u_{ramp}(t) = a + \frac{a}{T_{ramp}}(t - T_{ramp}) \quad (2)$$

$$u_{sin}(t) = b \sin(\omega_{sin}t) \quad (3)$$

$$I(t) = I_0[1 + mu_{ramp}(t) + mu_{sin}(t)] \quad (4)$$

In above equations, $u_{ramp}(t)$ and $u_{sin}(t)$ are the voltage of ramp signal and sine signal, a , b , m and T_{ramp} are the amplitude of ramp signal, the amplitude of sine signal, the intensity modulation coefficient and the cycle of ramp signal, respectively. The waveform of a standard ramp wave rises in a straight line, then falls sharply in one cycle period. In this paper, the cycle period of the modulating ramp wave was set as 10 Hz. The sine wave signal was set as 5 kHz. The sine wave signal is also set as the modulating signal and it is mounted on the ramp signal for modulation.

Therefore, the relationship of gas concentration and 2f harmonic signal of system can be calculated according to the equations. The ramp signal and the sine signal in above equations can be generated by DFB lasers which are under the control of the self-developed circuits.

MATERIALS AND METHODS

Laser driving circuit

According to the TDLAS technique, laser diode must be linearly controlled to scan across the gas absorption line. The driving current and operating temperature of laser diodes were precisely regulated using self-developed control circuits. Compared to the previous design, the main controller chip of the laser driving circuit was upgraded from TMS320F28335 to TMS320C28346. The main computing frequency reaches 300 MHz, with a cycle time of approximately 3.33 ns, resulting in a processing performance nearly twice that of the previous design. In this way, the floating-point performance has been enhanced and the algorithm for the detection system can be processed effectively especially for the digital lock-in part which involves complex real-time computing. Meanwhile, the TMS320C28346 also has abundant on-chip peripherals including six 32-bit timers, nine 16-bit timers, 258K 16-bit SARAM and serial port peripherals. However, there is also a problem of the new MCU in the system. Its package type is 256-ball plastic ball grid array (BGA) which is not convenient for hand soldering. After several attempts, the chip was successfully soldered on the board by using a hot air gun. The board has four layers as shown in Figure 3(a) which are top layer, bottom layer and two internal power layers. The completed board is shown in Figure 3(b).

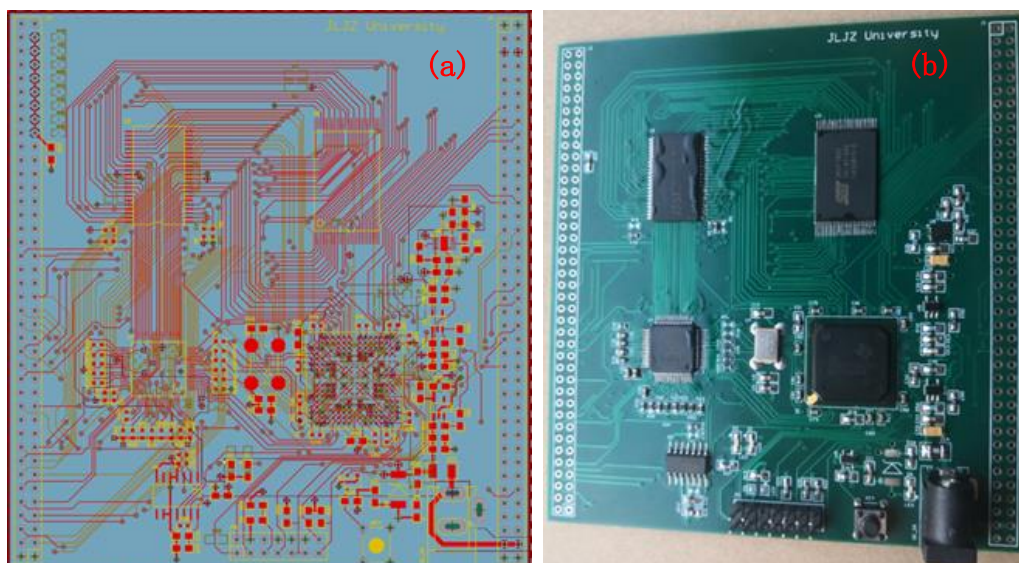


Fig. 3 – Self-developed PCB drawing (a) and soldered circuit board of the main controller

Laser temperature controller

The DFB laser has the characteristic that its output wavelength changes with the change of its operating temperature. Therefore, it is very important to control its operating temperature. On the one hand, if the temperature of the laser is too high, it may shorten its lifespan or cause damage to it. On the other hand, controlling the output wavelength of the laser by changing its temperature is very effective, especially in the detection system using TDLAS technology. Therefore, in this paper, a temperature control circuit for the DFB laser is developed based on the Thermoelectric Cooler (TEC) control circuit. The DFB laser used in the system has a built-in TEC module. Therefore, through the TEC control circuit, real-time and precise control of the laser's temperature can be achieved, thus enabling effective control of its output wavelength. The TEC control chip used in the system is the ADN8831. This chip can effectively control the TEC built into the laser based on the Analog PID algorithm. It can achieve a temperature fluctuation of no more than 0.01 degrees Celsius at the minimum. The photo of the developed circuit is shown in the figure. It is a four - layer PCB. The inner layer is the power layer, and the top and bottom layers are the signal layers. The compensation network of the laser diode is shown in Fig. 4. The resistors of R_{LOW} , R_{MID} and R_{HIGH} can be obtained in datasheet. The voltage V_{SET} , which decides the value of laser temperature, can be obtained by Eq. (5) - (8), as:

$$V_{SET} = \left(\frac{R_3}{R_{TH} + R_2} - \frac{R_3}{R_1} + 1 \right) \times \frac{V_{REF}}{2} \tag{5}$$

$$R_1 = R_{MID} + \frac{R_{MID}(R_{LOW} + R_{HIGH}) - 2R_{HIGH}R_{LOW}}{R_{HIGH} + R_{LOW} - 2R_{MID}} \tag{6}$$

$$R_2 = R_1 - R_{MID} \tag{7}$$

$$R_3 = \frac{R_1(R_1 + R_{LOW} - R_{MID})}{R_{LOW} - R_{MID}} \tag{8}$$

where V_{SET} is the output voltage for setting the temperature and it is can be set by DSP. The resistors of R_{LOW} , R_{MID} and R_{HIGH} set the temperature range which can be determined by specific characters of the laser diodes according to its datasheet, R_{TH} is the resistance of thermistor which is inside the DFB laser diode, V_{REF} is the reference voltage which is 2.5 V generated by the TEC controller chip, R_1 and R_2 are calculated by Eq. (6) and Eq. (7), R_3 represents the compensation resistor and can be calculated by Eq. (8). By using the above equations, as the resistors are chosen, the controlling voltage can be calculated and be generated to control the laser temperate.

The temperature controlling circuit is shown in Figure 4. In this circuit, the resistors and capacitors set the compensation network based on Analog PID. The temperature compensation network composed of these components can effectively approximate the actual value to the set value of temperature. The compensation network in the lower right corner can change the values of these resistors and capacitors by changing the jumper caps as shown in Fig. 4. The main controller chip of ADN8831 is placed on the center location of the board as shown in the photo. The left zone which is selected by the red lines is the temperature setting zone. The temperature value can be set by using serial resistors after calculation. The bottom area of the board is the compensation zone. The resistors and capacitors can be selected by using the jumper cap. According to the Analog PID algorithm, if the response time of the temperature controlling for DFB laser is extremely fast, the stability of the temperature fluctuation will be impacted. Therefore, it is necessary to achieve the balance of stability and response speed by adjusting the components.

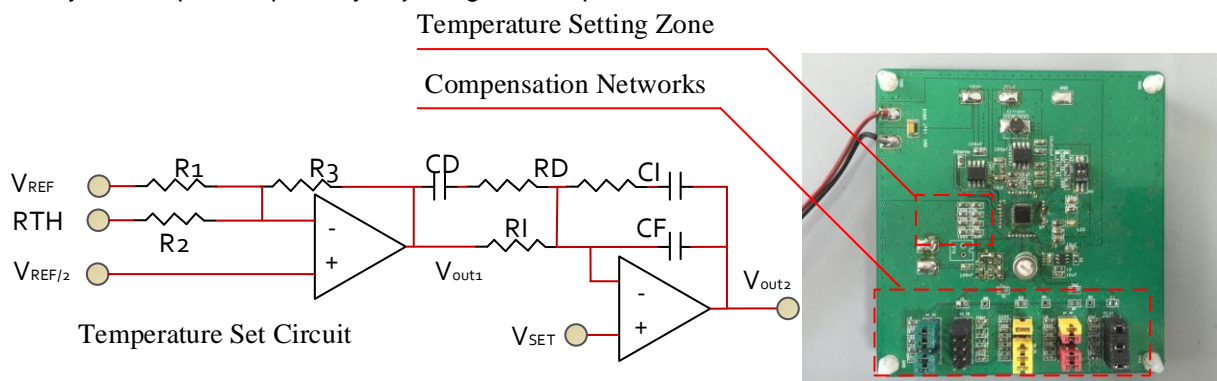


Fig. 4 – Temperature control circuit for DFB laser diode based on Analog PID algorithm

Experiments were carried out to investigate the temperature control performances by using the developed circuit. The stability test of the temperature control module is shown in Fig. 5.

The laser's temperature was stabilized at 24.55 °C within 15 hours. The laser temperature was sampled by an Analog-to-digital circuit. During the experiment, a random period of 100 minutes was selected to show the detailed fluctuation. Then, temperature data was transmitted by the serial port circuit from the DSP board to a computer. The fluctuation of temperature can determine the stability of the laser. The relationship between laser temperature and its output spectroscopy can be determined by carrying out experiments and be expressed as fitting formulas. The small temperature fluctuation within the range of ± 0.02 °C will not affect the stability of the output wavelength. Therefore, the fabricated laser temperature control circuit can effectively control the output wavelength of the laser.

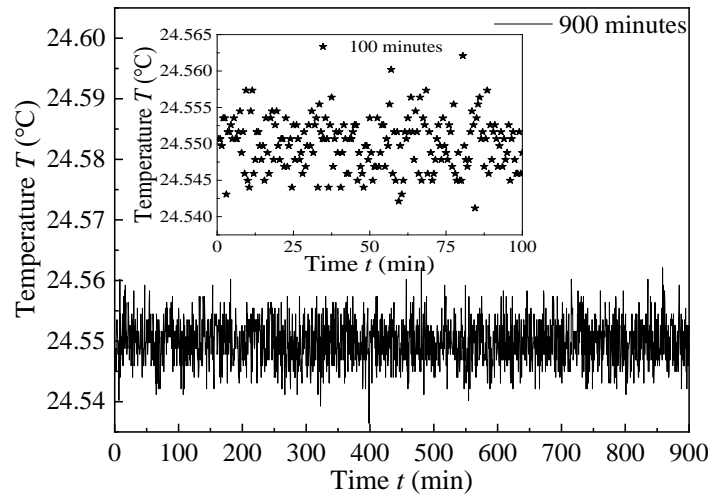


Fig. 5 – Temperature stability test of the proposed control circuit during 15 hours

HC-PCF characteristics

The Hollow-core photonic crystal is applied in this system. It can be used not only for signal transmission but also as a gas cell. The effective wavelength range of the HC-PCF used in the system is 1490-1680. Since the absorption peak of the gas to be measured in the system is around 1654 nm, the optical signal output by the laser can pass through the HC-PCF almost without loss. The transmission loss is only 25 dB/km. Its cross-section of the optical fiber is shown in Fig. 6(a). The center-to-center distance of the holes is 3.8 micrometers. Due to its 95% hollow structural characteristics, the gas to be measured can be filled inside, so that it can fully come into contact with the optical signal. The diameter of the fiber is about 70 μm . Its coating material is acrylate which has a single layer.

The gas diffusion performance of the HC-PCF has been tested in the system. Place the HC-PCF in a gas chamber with dynamic gas mixing, and inject methane gas with a concentration of 2000 ppm into the gas chamber through the method of dynamic gas mixing. Through observation, it can be seen that after approximately 69 minutes, the methane concentration inside the optical fiber is consistent with the external concentration. The speed of gas diffusion is acceptable for experiments such as long-term outdoor monitoring of methane. If it is necessary to increase the diffusion speed, laser drilling can be used to make holes in the outer sheath of the optical fiber. However, it is also necessary to re-evaluate the loss rate of its optical signal at the same time.

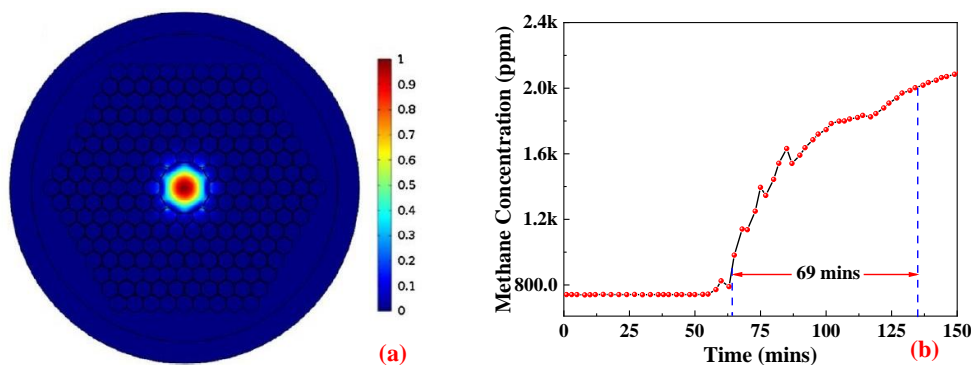


Fig. 6 – Simulation test of the optical structure (a) and the diffusion test of standard gas (b)

RESULTS AND DISCUSSIONS

Spectroscopy test

In order to meet the detection requirements of the detection system, the output spectrum of the laser must be stable and controllable. The output spectrum of the laser is determined by its control temperature and current. Therefore, it is important to evaluate the output spectral characteristics of the laser by changing its control temperature and driving current. The control temperature of the laser can greatly affect the output spectrum of the DFB laser, which is determined by the internal structure of the DFB laser. In contrast, the change in wavelength caused by the control current of the DFB laser is smaller than that caused by the control temperature. Therefore, during the experiment, it is usually the case that the output wavelength is first positioned at the absorption peak of the gas by changing the control temperature of the laser. Then, the wavelength position is finely adjusted by regulating the current of the DFB laser, so as to meet the requirements of the TDLAS detection technology.

In this paper, the proposed circuit controls the wavelength and the wavelength was tested by using an infrared spectrometer as shown in Fig.7. As can be seen in Fig.7(a), when the driving current of the laser is constant and the control temperature of the laser is changed, its central wavelength changes linearly. The injection current of the laser is set to 70 mA, and the adjustment coefficient between the temperature and the wavelength is approximately 0.115 nm/°C. In contrast, when the control temperature of the laser is kept constant, the driving current is changed, and the five sets of measured data are shown in Fig.7(b). The DFB circuit controls its current, which is increased from 40 mA to 80 mA with a step size of 10 mA. As shown in the figure, when the temperature of the laser is constant, the current of the laser is changed, and the adjustment coefficient between the current and the wavelength is measured to be approximately 0.014 nm/mA. Therefore, the control circuit proposed in this paper can effectively control the temperature and current of the laser, thus achieving effective control of its output wavelength and meeting the requirements of the detection system.

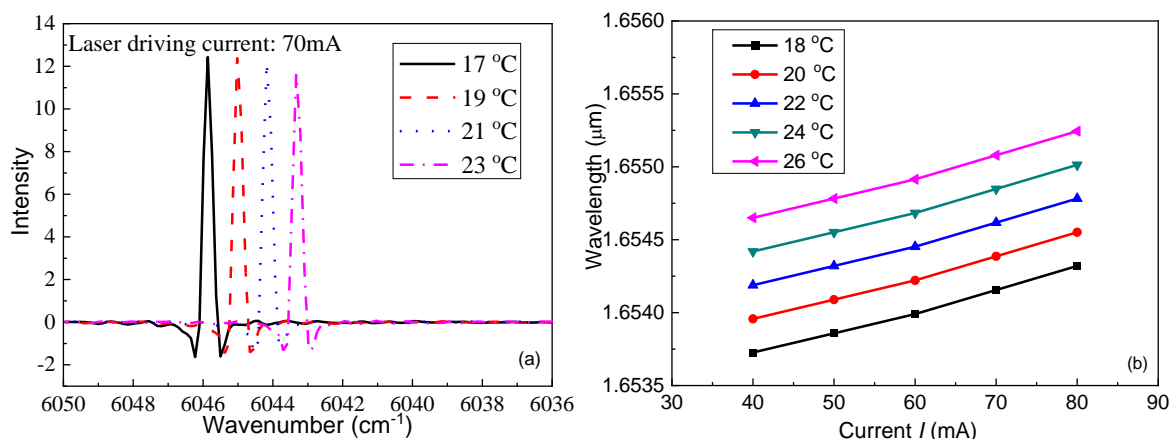


Fig. 7 – Spectroscopy test under the condition of constant temperature (a) and constant current (b)

Response time test

Since the detection and processing speed of infrared gas detection is very fast, the response time of the system is mainly determined by the volume of the gas chamber and the flow rate of the gas distribution. The detection system can detect the change of the concentration in the gas chamber in real time, so the data acquiring time of the DSP chip can be considered as the response time of the system. The calculation time of the DSP chip is very fast and the key signal which can be represent gas concentration can be obtained instantly. Compared to the traditional sensors, TDLAS technique has the advantage of fast response. This TDLAS based detection system performs an average calculation on the measured gas concentration, and the obtained average gas concentration is displayed on an LCD screen every 2 seconds. When the gas concentration in the gas chamber is changed, the fluctuation of the gas concentration will cause the detected second harmonic to fluctuate, as shown in Figure 8.

A gas mass flowmeter is applied in the system and it is required to manually adjust the knob to change the concentration during the process of gas detection. By adjusting the concentration, there is a certain slope at the rising edge of the concentration. Compared to the traditional method of gas distribution, dynamic gas distribution is the method that has better accuracy. The specific gravities of different gases need to be calculated and used to adjust the mass flowmeter in the experiment. When the target concentration is quickly

reached, the gas concentration in the gas chamber fluctuates as shown in Figure 8. Continuing to adjust the concentration when the concentration is not yet stable will cause the concentration of the gas chamber to oscillate. By measuring the Peak-to-Peak Voltage (PPV) value of the second harmonic, real-time fluctuations in gas concentration can be obtained.

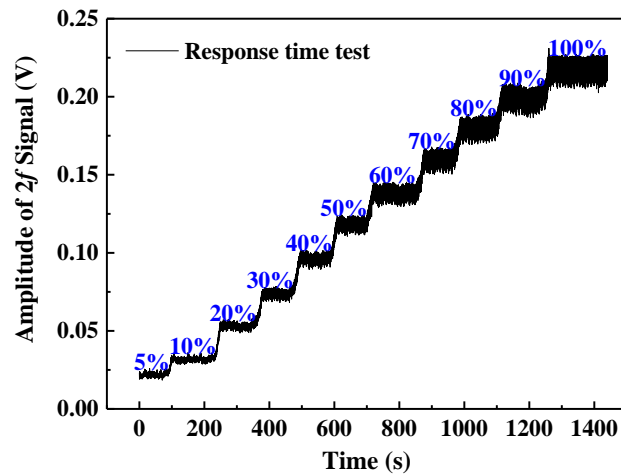


Fig. 8 – Response time test of the proposed detection system using 2f harmonic signal

Error test

The detection error of the detection system can be evaluated by using the dynamic gas mixing method. The dynamic gas mixing method can keep the gas concentration in the gas chamber approximately constant, and can change the gas concentration in the gas chamber within a short period of time. In the experiment, the high-concentration range and the low-concentration range were tested respectively, as shown in Fig. 9. For the experiments using high concentration of methane gas, the N₂ and pure CH₄ gas was mixed together after calculation of their relative height and volume. For the low concentration experiments, the pure liquid methane will be replaced by 1% standard gas to guarantee accuracy. In the high-concentration range, the error is relatively small, which is because the concentration inside the gas chamber using the dynamic gas mixing method is relatively stable, as shown in Fig. 9(a). In the low-concentration range, the error increases as shown in Fig.9(b). By calibrating the gas concentration with the second harmonic, the detection sensitivity can be further enhanced.

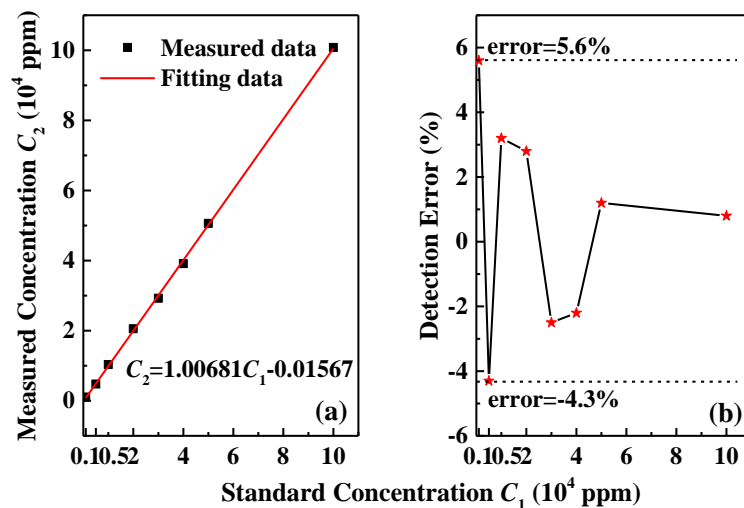


Fig. 9 – Error test of the measured methane gas using standard gas

Detection limit test

In combination with the WMS technology, detection sensitivity can be further improved. Through the sine wave and square wave of the same frequency and phase generated by the DDS, the first harmonic and the second harmonic after gas absorption can be obtained. Among them, the second harmonic can more effectively characterize the gas concentration, and the experiment carried out is shown in Fig.10.

In Fig.10(a), it can be seen that within the detection range, the second harmonic can be effectively extracted and is still clearly visible at 600 ppm. In Figure (b), when the gas chamber is filled with pure nitrogen, the fluctuation of the second harmonic can be evaluated, which is within the range of 1748 - 1754 mV. By increasing the effective absorption optical path, the detection lower limit of the system can be further reduced. In subsequent experiments, by using HC-PCF, the effective absorption optical path can be greatly increased, thereby improving the detection sensitivity of the system.

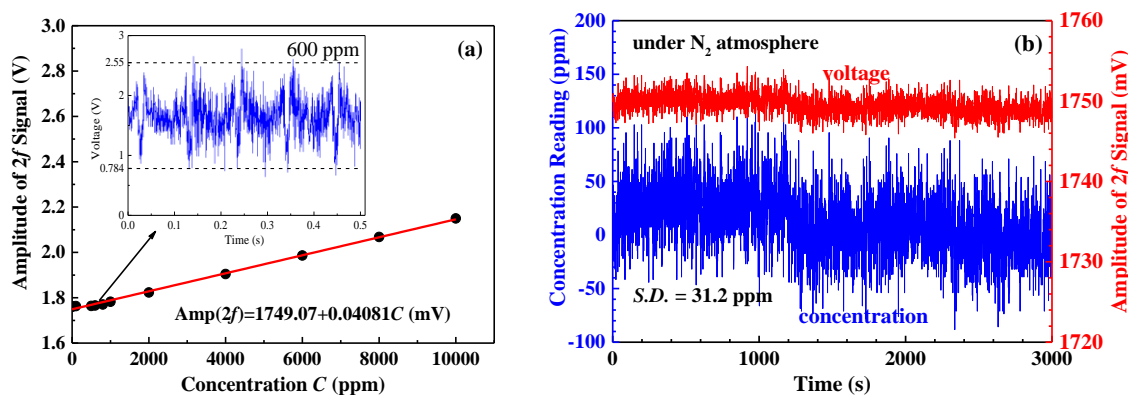


Fig. 10 – Detection limit test using 2f harmonic signal (a) and mixed standard gas (b)

CONCLUSIONS

The proposed methane detection system involves a DFB laser, InGaAs photodiodes, HC-PCF and updated circuits such as the DSP28346 circuit for laser controlling. By using the key components, the detection system has the ability to perform accurate remote detection of target gas. Through spectral testing, the stability of the laser's control temperature and driving current was verified, and the respective control coefficients were obtained. By conducting a variety of gas detection experiments, the effectiveness and stability of the detection system for detecting methane gas were developed. In subsequent research work, the use of HC-PCF will be increased to further improve the detection sensitivity of the detection system. Combined with this new type of optical fiber, the developed system can be used for large-scale methane gas monitoring in paddy fields.

ACKNOWLEDGEMENT

The authors wish to express their gratitude to Jilin Association for Higher Education (JGJX2020D246), the Education Department of Jilin Province of China (JKH20230334KJ), the Science and Technology Department of Jilin (20230203022SF, 20240302064GX), Changchun Development and Reform Commission (2022C045), and Undergraduate Innovation and Entrepreneurship Training Program Funding Project 2024 of Jilin Jianzhu University (S202410191078), for the generous support of this work.

REFERENCES

- [1] Arianti, F.D., Pertiwi, M.D., Triastono, J., (2023), Study of Organic Fertilizers and Rice Varieties on Rice Production and Methane Emissions in Nutrient-Poor Irrigated Rice Fields. *Sustainability*, vol.14, 5919. Switzerland; <https://doi.org/10.3390/su14105919>
- [2] Bai, Y.; Dai, Q.; Hai, J., Wang Q., Liao D., Liu G., Wang Y., Huang J., Zhang R., Siddig A. A. H., Bao W., Yang G., (2023), Manganese Slag Amendment Reduces Greenhouse Gas Emissions from Paddy Soil. *Atmosphere*, vol.14, 131. Switzerland; <https://doi.org/10.3390/atmos14010131>
- [3] Bai, Y.R., Yu H., He C., Miao Z., Rui D., Zhang Y., Lin X., (2021), A numerical simulation of a near-infrared three-channel trace ammonia detection system using hollow core photonic crystal fibre. *Optik*, vol.227, 166006, Germany; <https://www.sciencedirect.com/science/article/abs/pii/S0030402620318192?via%3Dihub>
- [4] Bin L., Shuocheng Z., Yaodan C., (2018), Development and Integration of a CO Detection System Based on Wavelength Modulation Spectroscopy Using Near-Infrared DFB Laser, *Journal of Spectroscopy*. vol.2018, 1707252, U.S.A.; <https://onlinelibrary.wiley.com/doi/10.1155/2018/1707252>
- [5] Catia, L., Sonia, O., P., Nelia, A., Maxime L., Mederic L., Florinda M. C., Joao L. P., Christophe C., Carlos M., (2021), Cortisol in-fibre ultrasensitive plasmonic immune-sensing. *IEEE Sensors Journal*, 21 (3), 3028-3034, U.S.A.; <https://ieeexplore.ieee.org/document/9201317>

- [6] Dar, S.A., Qazi, G, (2020), Investigation and comparison of sensitivity of LiDAR to laser physical parameters at 750 m using different detection techniques. *Optik*, vol.219, 165281, Germany; <https://www.sciencedirect.com/science/article/abs/pii/S0030402620311177?via%3Dihub>
- [7] Davis, N.M., Hodgkinson, J., Francis, D., Tatam R.P., (2016), Sensitive detection of methane at 3.3 μm using an integrating sphere and Inter-band Cascade Laser. *Optical Sensing and Detection IV*, vol.9899, 98990. Belgium; <https://www.spiedigitallibrary.org/conference-proceedings-of-spie/9899/1/Sensitive-detection-of-methane-at-33-%c2%b5m-using-an-integrating/10.1117/12.2227131.short>
- [8] Gao, Z.R., Ni, J.Z., Yan, J.Q., Jiang Q., (2018), Water-efficient sensing method for soil profiling in the paddy field. *International Journal of Agricultural and Biological Engineering*, vol.11(4), 207, China; <https://ijabe.org/index.php/ijabe/article/view/3593>
- [9] Jiao, Y.X., Fan, H.J., Gong, Z.F., Yang, K., Shen, F., Chen, K., Mei, L., Peng, W., Yu, Q., (2021), Trace CH₄ Gas Detection Based on an Integrated Spherical Photoacoustic Cell. *Applied Sciences*, vol.11, 4997, Switzerland; <https://www.mdpi.com/2076-3417/11/11/4997>
- [10] Jikun H., Yangjie W., (2014), Financing Sustainable Agriculture Under Climate Change. *Journal of Integrative Agriculture*, vol. 13, Issue 4, pp.698-712, China; <https://www.sciencedirect.com/science/article/pii/S209531191360698X?via%3Dihub>
- [11] Ma, J.L., Chen, W.Y., Niu, X.J., Fan Y.M., (2019), The relationship between phosphine, methane, and ozone over paddy field in Guangzhou, China. *Global Ecology and Conservation*, 17, U.S.A.; <https://www.sciencedirect.com/science/article/pii/S2351989418304955?via%3Dihub>
- [12] Maxime, L., Mederic, L., Marc, D., Karima C., Erik G., Christophe C., (2023), Electro-plasmonic assisted biosensing of proteins and cells at the surface of optical fibre. *Biosensors & Bioelectronics*, vol.220, 114867, England; <https://www.sciencedirect.com/science/article/abs/pii/S0956566322009071?via%3Dihub>
- [13] Mujiyo, M., Sunarminto, B.H., Hanudin, E., Widada J., Syamsiyah J., (2017), Methane production potential of soil profile in organic paddy field. *Soil Water Res*, vol.12(4), 212-219. Czech; https://www.agriculturejournals.cz/artkey/swr-201704-0004_methane-production-potential-of-soil-profile-in-organic-paddy-field.php?back=%2Fsearch.php?query%3DMethane%2Bproduction%2Bpotential%2Bof%2Bsoil%2Bprofile%2Bin%2Borganic%2Bpaddy%2Bfield%26sfrom%3D0%26spage%3D30
- [14] Palmer, P.I., Feng, L., Lunt, M.F., (2021), The added value of satellite observations of methane for understanding the contemporary methane budget. *Philosophical transactions of the royal society a-mathematical physical and engineering sciences*, vol.379, 20210106. England; <https://royalsocietypublishing.org/doi/10.1098/rsta.2021.0421>
- [15] Rajasekar, P., Selvi J.A.V., (2022), Sensing and Analysis of Greenhouse Gas Emissions from Rice Fields to the Near Field Atmosphere. *Sensors*, vol.22, 4141. Switzerland; <https://doi.org/10.3390/s22114141>
- [16] Rizzo, A., Boano, F., Revelli, R. (2015) Groundwater impact on methane emissions from flooded paddy fields. *Advances in water resources*, vol.83(Sep.), pp.340-350. U.S.A.; <https://www.sciencedirect.com/science/article/abs/pii/S0309170815001529?via%3Dihub>
- [17] Xie, B.H., Zhou, Z.X., Zheng, X.H., Zhang W., Zhu J.G., (2010), Modeling methane emissions from paddy rice fields under elevated atmospheric carbon dioxide conditions. *Advances In Atmospheric Sciences*, vol.27(1), 100-114, England, <https://link.springer.com/article/10.1007/s00376-009-8178-4>
- [18] Xu, X.Y., Zhang, M.M., Xiong Y.S., Yuan J.F., Shaaban M., Zhou W., Hu R.G., (2020), The influence of soil temperature, methanogens and methanotrophs on methane emissions from cold waterlogged paddy fields. *Journal Of Environmental Management*, vol.264, 110421. U.S.A.; <https://www.sciencedirect.com/science/article/abs/pii/S0301479720303558?via%3Dihub>
- [19] Zhang, G.B., Zhang, W.X., Yu, H.Y., Ma J., Xu. H., Yagi K., (2015), Fraction of CH₄ oxidized in paddy field measured by stable carbon isotopes. *Plant and Soil*, vol.389(1/2), pp.349-359, Netherlands; <https://link.springer.com/article/10.1007/s11104-014-2365-5>
- [20] Zhang, G.B., Ji, Y., Liu, G., Ma J., Xu H., (2014), Carbon isotope fractionation during CH₄ transport in paddy fields. *Science China - Earth sciences*, vol.57(07), pp.1664-1670, China; <https://link.springer.com/article/10.1007/s11430-014-4879-3>